Journal of the European Ceramic Society **12** (1993) 353–360

Pressing and Sintering Behaviour of Yttria Stabilized Zirconia Powders Prepared from Acetate Solutions

A. Samdi,[a,b] B. Durand,[a] M. Roubin,[a] A. Daoudi[b]

[a] Laboratoire de Chimie Minérale 3, URA CNRS No. 116, ISIDT, Université Claude Bernard, Lyon I.
43 Boulevard du 11 Novembre 1918, 69622 Villeurbanne Cedex, France
[b] Faculté des Sciences Aîn Chok, Université Hassan II, km 8, Route d'El Jadida, B.P. 5366, Maârif, Casablanca, Morocco

M. Taha, J. Paletto & G. Fantozzi

GEMPPM, INSA de Lyon, URA CNRS No. 341, 69621 Villeurbanne Cedex, France

(Received 7 October 1992; revised version received 9 June 1993; accepted 24 June 1993)

Abstract

Yttria stabilized zirconia powders (3 mol% in Y_2O_3) were prepared by the drying and air-calcination of amorphous gelatinous precipitates obtained by hydrolysis of solutions containing both zirconium and yttrium acetates. After sintering in air at 1500 or 1600°C, the characteristics of the materials were correlated with certain of the synthesis parameters (concentration of starting solution and neutralizing agent). Cold pressing compaction curves are analysed and the influence of residual oxycarbonates or carbonates on sintering is discussed.

Durch yttrium oxid (3 mol% Y_2O_3) stabilisierte Zirkoniumpulver sind mittels Trocknung und Kalzinierung an Luft aus gelatineartigen und amorphen Niederschlägen hergestellt worden. Diese Niederschläge wurden durch Hydrolyse von Azetatlösungen mit teils Zirkonium, teils Yttrium gewonnen. Nach dem Sintern an der Luft, bei 1500 oder 1600°C, korrelieren die Materialeigenschaften mit einigen Herstellungsparametern (z. B. Konzentration der Anfangslösung und Neutralisierungszusatz). Wir haben ebenfalls die Graphen der kaltpressung analysiert, gleichwie den Einfluß von behalteten Oxidkarbonaten und Karbonaten auf die Sinterung.

Des poudres de zircone stabilisée à l'oxyde d'yttrium (3 mol% Y_2O_3) sont préparées, par séchage et calcination à l'air, de précipités gélatineux et amorphes obtenus par hydrolyse de solutions d'acétates de zirconium et d'yttrium. Après frittage à 1500 ou à 1600°C, les caractéristiques morphologiques des matériaux frittés sont corrélées avec quelques paramètres de synthèse (concentration de la solution de départ et de l'agent neutralisant). Nous avons aussi analysé les courbes de compaction à froid ainsi que l'influence d'oxycarbonates ou de carbonates résiduels sur le frittage.

1 Introduction

The physical characteristics of sintered ceramics greatly depend upon the morphology of the starting powders and consequently on the method used for their synthesis. Thus, various synthesis methods have been investigated.[1–4]

It was recently shown in the authors' laboratory that pure[5,6] or yttrium stabilized zirconia[7] powders could be formed by pyrolysis of acetate precursors, the preparation procedure of the precursor having a strong influence on the morphology of the powders.

Following this earlier study, the present paper is concerned with the analysis of relations between certain of the synthesis parameters and the behaviour of yttrium stabilized zirconia powders during cold pressing compaction and natural sintering.

Journal of the European Ceramic Society 0955-2219/93/$6.00

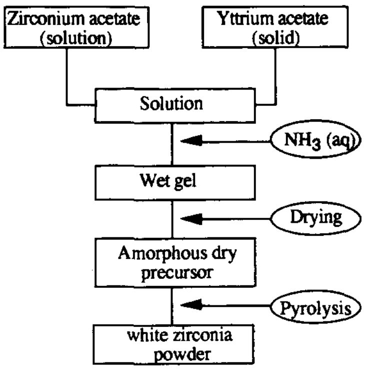

Fig. 1. Powder preparation flow chart.

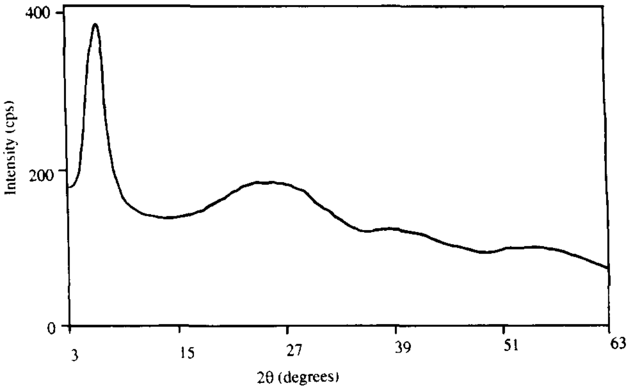

Fig. 2. X-Ray pattern of dried gel C.

2 Preparation and Characterization of Powders

2.1 Precursor preparation

The zirconium source was a commercial solution of zirconyl acetate containing 22 wt% ZrO_2 (Riedel de Haen). Stabilizing yttrium was provided by yttrium acetate prepared by dissolving yttrium oxide (Merck) in a 1/1 water–pure acetic acid solution and evaporating to dryness on a sand bath at 80–90°C.

Zirconia, stabilized with 3 mol% Y_2O_3 (ratio $Y_2O_3/[Y_2O_3+ZrO_2]$), was prepared from gels formed by the hydrolysis of zirconyl acetate solutions in which solid yttrium acetate was dissolved, according to the flow chart presented in Fig. 1.

Hydrolysis is carried out by ammonia addition until a hydrolysis ratio of $r = 0{\cdot}9$ is reached (r = moles of OH^- added/initial moles [Y + Zr]). At this ratio, the viscosity of the gel is such that it can no longer be stirred. Gels were then dried on a sand bath at 80–90°C for 15 h. X-Ray diffraction patterns indicate amorphous powders (Fig. 2). The synthesis conditions for the gels are summarized in Table 1.

2.2 Experimental

Pyrolysis of the dry gels was investigated by thermogravimetric analysis (TGA) using a SETARAM device (TG-DTA 92) coupled to a quadrupole mass spectrometer (Balzer) allowing the identification of released gases.

X-Ray diffraction patterns recorded by means of a Siemens D500 automatic diffractometer working with CuK_α radiation. The size of crystallites was estimated according to the Scherrer method after correcting for experimental errors by using a parabolic law.[8]

The mean size of agglomerates was obtained using a Horiba CAPA 500 granulometer with a centrifugating device. Powders are dispersed in deionized water made basic to pH = 9 and containing 1 wt‰ sodium polymethacrylate. The conditions leading to optimal dispersion were stated previously.[9]

The porosity of compacts was estimated before and after sintering by means of a mercury porosimeter (Carlo Erba 2000) reaching 2000 bars and allowing the characterization of pores in the range 3·75–7500 nm. Green density was calculated from the measurement of the diameter and the thickness of the pellets. The density of sintered materials was measured by Archimedes' method. Relative density is based on a theoretical value of 6100 kg/m^3 for 3 mol% yttrium stabilized zirconia. Specific surface area was measured by the BET method.

Compaction tests were carried out on a mechanical test machine (Instron 1195 apparatus) from 0 to 200 MPa with a crosshead rate of 0·5 mm/min. The tap density is achieved before beginning compaction according to the AFNOR normalization.[10] Density variation during pressing was deduced from the crosshead continuous displacement. Deviation due to the elastic deformation of the load was evaluated by taking into account a blank test without powder

Table 1. Synthesis parameters

$C_0 = [Zr+Y]_0$ *initial concentration (mol/litre)*	*[NH3] concentration (mol/litre)*	$C_{gel} = [Zr+Y]_{gel}$ *(mol/litre)*	*pH*	*Dried gel identification*
0·55	0·5	0·28	6·4	A
2·75	0·5	0·50	6·4	B
2·75	1·3	0·98	6·6	C
2·75	2·2	1·29	6·7	D
2·75	2·8	1·44	6·6	E
2·75	3·8	1·63	6·9	F

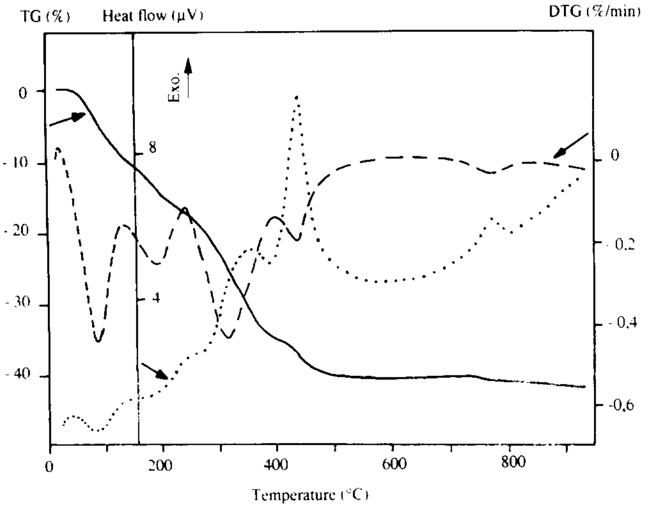

Fig. 3. Thermal analysis of dried gel C: ———, thermogravimetric data (TG); – – – –, derivative of thermogravimetric data (DTG); ·······, differential scanning calorimetry data (heat flow; HF).

in the die and by recording the response over the same pressure range.

Sintering was performed with a dilatometer, Adamel DI24, using a 1°C/min heating rate, a hold at the final temperature for 3 h and a cooling rate of 2 C/min to room temperature.

2.3 Thermal behaviour of dry gels

The pyrolysis of dry gels in air up to 900°C at a rate of 150°C/h occurs with the same steps for all samples (Fig. 3 and Table 2). The decomposition began near 50°C and seemed to end at about 530°C. Gels are dehydrated in two steps as shown by the two endothermic peaks on the DSC curves (100 and 200°C). The decomposition of acetate groups is exothermic; it occurs between 245 and 400°C and involves the release of dimethyl acetone, carbon dioxide and water vapour. Acetone can be formed by dismutation of acetate ions:

$$2CH_3COO^- \rightarrow (CH_3)_2CO + CO_3^{2-}$$

Beyond 400°C, the decomposition of carbonate or oxycarbonate groups is shown by an exothermic peak. However, the black colour of the residue obtained at 530°C indicates that carbon is not completely eliminated and it was necessary to heat to 900°C to obtain white tetragonal zirconia. A second exothermic peak between 750 and 800°C and a small weight loss were observed, corresponding to the release of a mixture of CO_2 and H_2O.

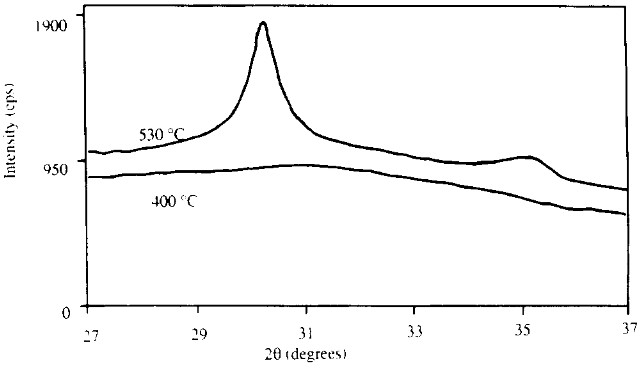

Fig. 4. X-Ray pattern of dried gel C calcined in air at 400 and 530°C.

X-Ray diffraction identification of the pyrolysis residue at different temperatures (Fig. 4) agreed with the following process:

$$\text{Dry gel} \xrightarrow{400^{\circ}\text{C}} \begin{matrix}\text{Amorphous}\\ \text{ZrO}_2\end{matrix} \xrightarrow{530^{\circ}\text{C}}$$

$$\begin{matrix}\text{Black}\\ \text{tetragonal ZrO}_2\end{matrix} \xrightarrow{900^{\circ}\text{C}} \begin{matrix}\text{White}\\ \text{tetragonal ZrO}_2\end{matrix}$$

2.4 Morphological characteristics of zirconia powders formed by pyrolysis up to 900°C

For the tetragonal zirconia powders obtained, an increase in the ammonia concentration and consequently in the concentration of zirconium and yttrium in the reaction medium (C gel), decreased the size of agglomerates but had no influence on the size of crystallites (Table 3). According to the size of the agglomerates, samples were divided into two groups characterized respectively by mean diameters close to 3·5 µm (C900, D900, E900 and F900) and to 5·5 µm (A900 and B900), as shown in Fig. 5.

The mean size of crystallites, estimated from X-ray broadening, was always close to 20 nm. The size would equate with a surface area of 50 m^2/g, that is to say ten times larger than the one calculated from nitrogen adsorption data. Consequently it can be

Table 2. Investigation of the pyrolysis of gel C (heating rate in air 150°C/h)

Temperature (°C)	*Gaseous release analysis*	*Weight loss (%)*	*Thermal effect*
50–135	H_2O	9·1	endothermic
135–245	H_2O	7·9	endothermic
245–400	$(CH_3)_2CO + CO_2 + H_2O$	17·3	exothermic
400–530	$CO_2 + H_2O$	4·6	exothermic
530–740	—	0·0	—
740–940	$CO_2 + H_2O$	2·5	exothermic

Table 3. Morphological characteristics of tetragonal zirconia samples

Sample	*Crystallite mean diameter (nm)*	*Specific surface area (m²/g)*	*Agglomerate mean diameter (µm)*
A900	19·5	5	5·7
B900	20·0	6	5·4
C900	20·5	6	3·6
D900	20·0	6	3·5
E900	20·5	6	3·6
F900	20·0	4	3·3

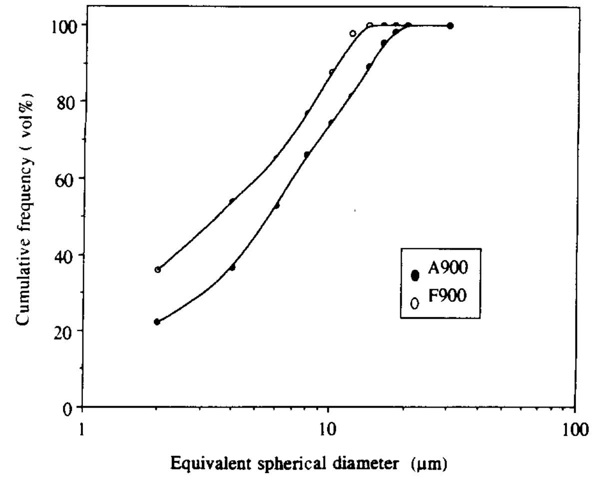

Fig. 5. Agglomerate size in samples A900 and F900; cumulative frequency curves.

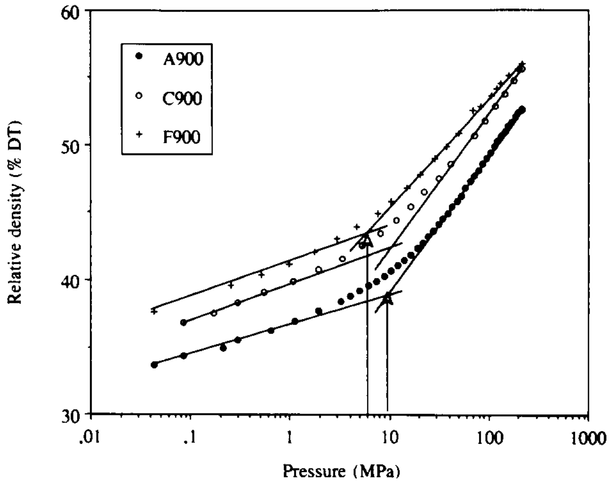

Fig. 7. Green density versus compaction pressure for powders A900, C900 and F900.

unambiguously concluded that elementary grains are polycrystalline. The measured area, 6 m^2/g, is consistent with spherical elementary grains exhibiting a diameter of about 0·15 μm. Some elementary grains have been isolated on TEM micrographs. The one shown in Fig. 6 is perfectly consistent with this latter size if it is assumed that its equivalent diameter is the half sum of the length and of the width. Moreover, it can be seen that the elementary grains are formed by the sintering of crystallites with sizes close to the one estimated from X-ray broadening.

3 Compaction and Sintering of Zirconia Powders

3.1 Compaction

In order to estimate the hardness of the agglomerates and the compaction rate of powders, samples A900, C900 and F900 were uniaxially cold pressed up to 200 MPa. As shown in Fig. 7, compaction data for the powders can be fitted[11–15] to two linear sections when plotted as logarithm of pressure versus percentage density.

In the low pressure region, densification is attributed to rearrangement of agglomerates in the matrix, controlled according to Van de Graaf *et al.*[12] by particle–particle friction. The break point (P_j) shows the beginning of agglomerate fracture; it was characteristic of their hardness and gave a good indication of the compression strength of the powder agglomerates.[12] At pressures exceeding P_j, densification can be attributed to the elimination of intergranular porosity, as suggested by Dimilia & Reed.[15] The slope of the density versus logarithm of pressure curve is also an important parameter for powder pressing and indicates the efficiency of pressing.[16]

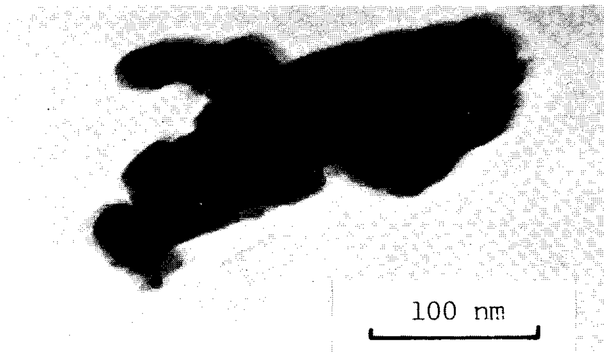

Fig. 6. TEM micrographs of starting powder B900.

From the three samples investigated, it can be concluded that the agglomerates became more dense in the sequence A900, C900, F900 as their size decreased. Samples A900 and C900 exhibited the break point P_j at pressures close to 10 MPa, whereas, for sample F900, P_j occurred at 6 MPa. Thus, sample F900 should appear as the most easily compactable, but when the pressure exceeded P_j, it was characterized by a lower slope. The same density, about 55% of the theoretical, was obtained for samples C900 and F900 when the pressure reached 250 MPa. Comparing the three samples, the increase of tap density involved a linear decrease of the slope of the compaction curves for pressures above P_j (Table 4, Fig. 8).

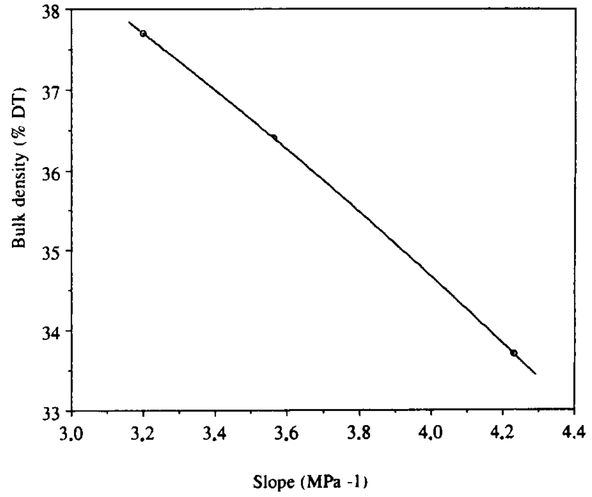

Fig. 8. Variation of the bulk density of samples A900, C900 and F900 versus slope of compaction curves when $P > P_j$ (Fig. 5).

Table 4. Compaction data

Sample	*Tap density (% TD)*	*Break point pressure P_j (MPa)*	*Slope ($P > P_j$) (% TD) (MPa^{-1})*	*Density at 200 MPa (% TD)*
A900	33·7	10	4·23	52·7
C900	36·4	10	3·56	54·9
F900	37·7	6	3·20	55·6

Similar behaviour has been found in powders prepared by the hydrolysis of metal alkoxides[12] ($P_j = 30$ MPa, relative agglomerates density = 33%). On the other hand, no break point was noticed in compaction curves of zirconia prepared from citrate, which formed tissue-like two-dimensional agglomerates.

3.2 Sinterability

The dilatometric study was performed with compacts obtained by cold pressing, first uniaxial up to 100 MPa and then isostatic up to 400 MPa.

On heating up to 900°C, the dilatometric curves of all samples (Fig. 9) gave only small expansions because dilatation was accompanied by a release of superficial adsorbed water, as is corroborated by thermogravimetric investigation of the compacted samples, which showed a first weight loss between 200 and 500°C (Fig. 10). Beyond 900°C, sintering occurred continuing even at 1500°C, as shown on the isothermal curves (Fig. 11). A second weight loss, involving dedensification in competition with sintering, occurred simultaneously (Fig. 10). It corresponded to the decomposition of residual carbonate or oxycarbonate groups. Such a phenomenon was observed previously and with a greater intensity for yttrium-containing zirconia prepared from acetate solution using a different procedure.[17] The consequences of the elimination of residual volatile materials on sintering have been discussed by different authors.[18–22]

Increase of sintering temperature from 1500 to 1600°C increases the linear shrinkages and the sintered densities except for sample F900 (Table 5). The best results were obtained for samples D900 and E900 characterized by a shrinkage of 12% and a

Table 5. Sintering data

Starting powder	*After sintering at 1500°C for 3 h*		*After sintering at 1600°C for 3 h*	
	Density (% TD)	*Shrinkage (%)*	*Density (% TD)*	*Shrinkage (%)*
A900	72·5	12·8	80·3	13·6
B900	74·1	12·9	82·0	13·5
C900	79·0	11·9	84·8	12·7
D900	77·4	11·7	85·2	12·5
E900	78·7	11·9	84·9	12·5
F900	75·4	11·7	76·6	11·6

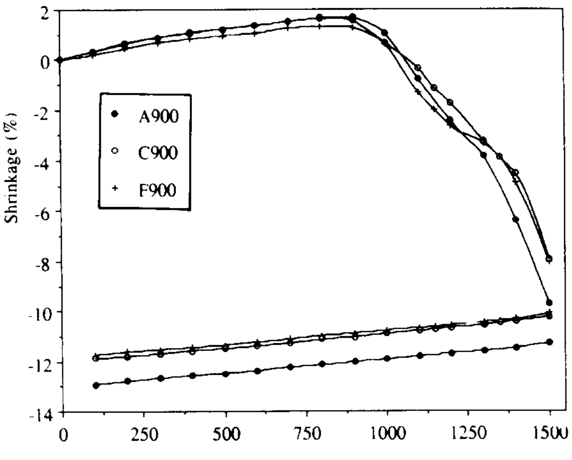

Fig. 9. Dilatometric curves of samples A900, C900 and F900.

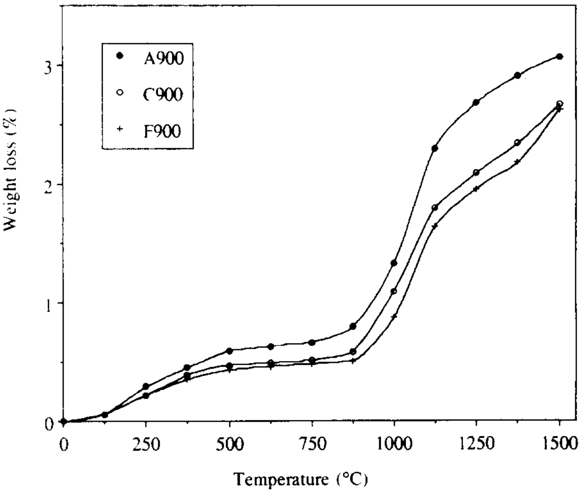

Fig. 10. Thermogravimetric behaviour of samples A900, C900 and F900 compacted at 400 MPa.

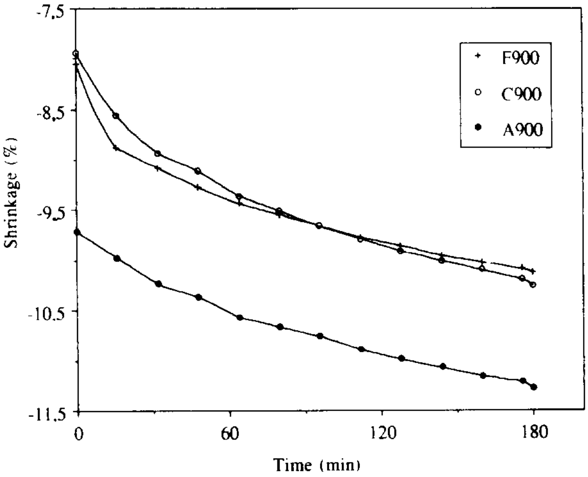

Fig. 11. Isothermal dilatometric curves of samples A900, C900 and F900.

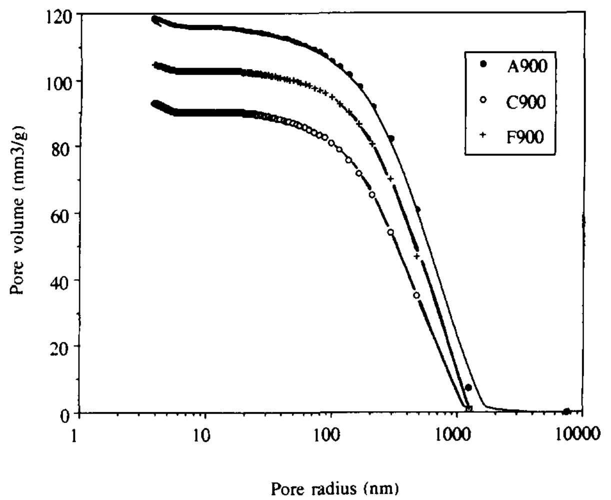

Fig. 12. Mercury penetration curves versus pore radius of samples A900, C900 and F900 compacted at 400 MPa.

Table 6. Porosity of compacted powders

Starting powder	*Isostatic pressing at 400 MPa*		
	Green density (% TD)	*Open pores volume (mm^3/g)*	*Open pores radius (nm)*
A900	55·1	122·5	30–3000 < 10
B900	55·9	112·7	30–3000 < 10
C900	56·4	94·3	30–2000 < 10
D900	57·4	97·5	30–2000 < 10
E900	57·4	95·1	30–2000 < 10
F900	54·3	104·8	30–2000 < 10

final density 85% of the theoretical. It must be noted that after sintering, destabilization of the tetragonal phase during cooling was never observed.

3.3 Microstructures of dense materials

3.3.1 Green materials

Mercury penetration curves of the green compacts (Figs 12 and 13, Table 6) showed interagglomerate porosity in the diameter range 30 to 3000 nm for samples A900 and B900, and 30 to 2000 nm for samples C900, D900, E900 and F900. Of the latter group, the first three exhibited porous volumes close to 95 mm^3/g whereas F900 showed a greater volume, involving a decrease of green density. Samples A900 and B900 were also characterized by a large porous volume.

The mercury penetration curves (Fig. 12, Table 6) also showed a small intraagglomerate porosity of size smaller than 10 nm.

After cold isostatic pressing at 400 MPa, the measurement of green density showed that sample F900 was less compacted than D900 and E900, whereas, by uniaxial pressing at 200 MPa, it gave the best results (Table 4, Fig. 7). This apparently surprising behaviour is explained by the decrease of slope of the curve of density versus logarithm of pressure for pressures exceeding P_j when the bulk density of the sample increased.

3.3.2 Sintered materials

For all green samples, sintering at 1500°C for 3 h involved the disappearance of the intraaggregate porosity, but large intraaggregates pores still remained. Compared to green samples, the distribution of pore sizes in sintered samples always

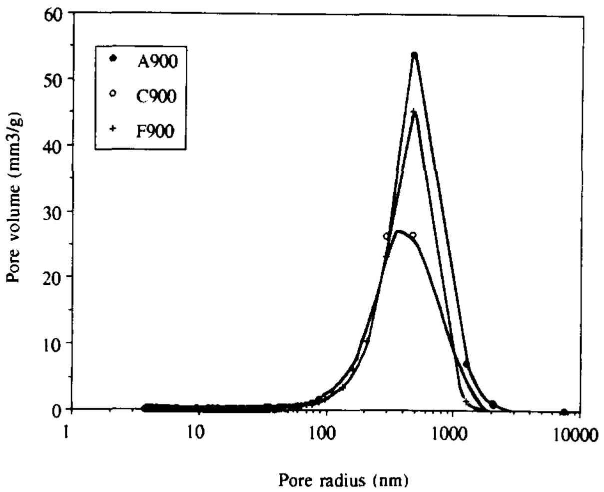

Fig. 13. Pore size distribution of samples A900, C900 and F900 compacted at 400 MPa.

Table 7. Porosity of sintered materials

Starting powder	*1500°C (3 h)*		*1600°C (3 h)*	
	Open pores volume (mm^3/g)	*Pores radius (nm)*	*Open pores volume (mm^3/g)*	*Pores radius (nm)*
A900	56·6	830–7500 130–830	37·6	830–7500 150–830
B900	53·2	830–7500 130–830	33·2	830–7500 180–830
C900	33·1	130–580	23·5	150–580
D900	34·3	130–680	23·1	140–830
E900	36·2	130–680	22·5	140–830
F900	50·3	130–830	49·3	170–2500

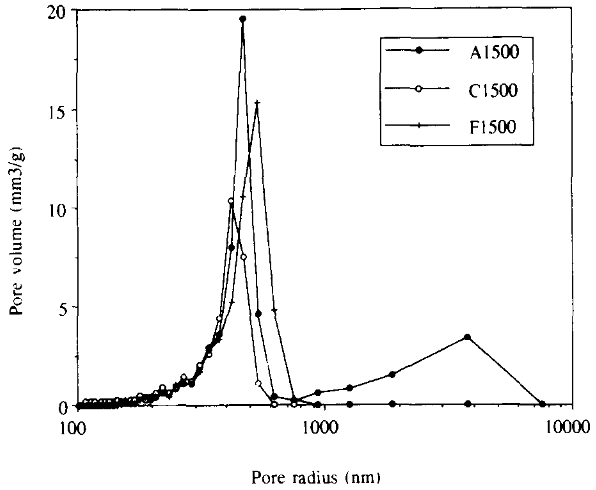

Fig. 14. Pore size distribution of samples A1500, C1500 and F1500 sintered at 1500°C for 3 h.

became narrower and shifted towards smaller values (Table 7, Fig. 14). For example, green sample D900 gave sizes in the range 30 to 2000 nm and sintered ones in the range 130 to 680 nm. In samples A900 and B900, a second family of pores was found in the 830 to 7500 nm range. Such pores were larger than the ones present in the green materials. For these two samples, the weight loss occurring beyond 1000°C (Fig. 11) was greater than for the other samples.

The increase of sintering temperature from 1500 to 1600°C brought only a very small change in the pore size distributions, but the porous volume decreased (Table 7). A small degree of grain growth was simultaneously observed at 1600°C (Fig. 15).

Scanning electron micrographs of materials sintered at 1500°C for 3 h corroborated the existence of macroporosity and intraaggregate homogeneous sintering (Fig. 16).

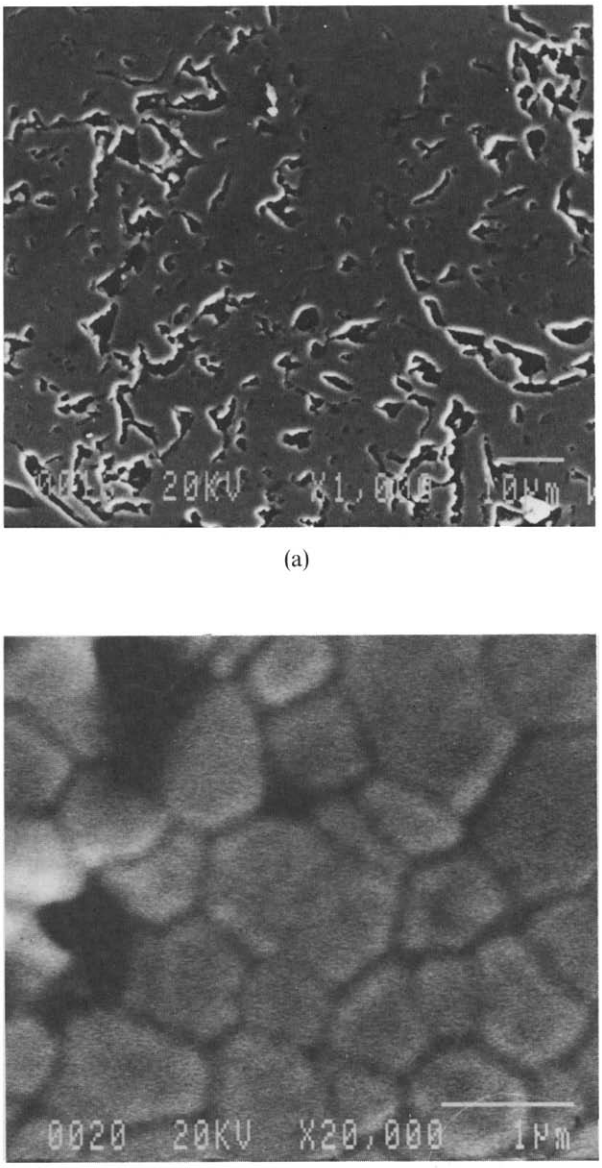

(a)

(b)

Fig. 15. SEM micrographs of polished surface of sample A900 sintered for 3 h at 1600°C: (a) showing an intergranular porosity; (b) showing an intraaggregate homogeneous sintering and a small growth of grains.

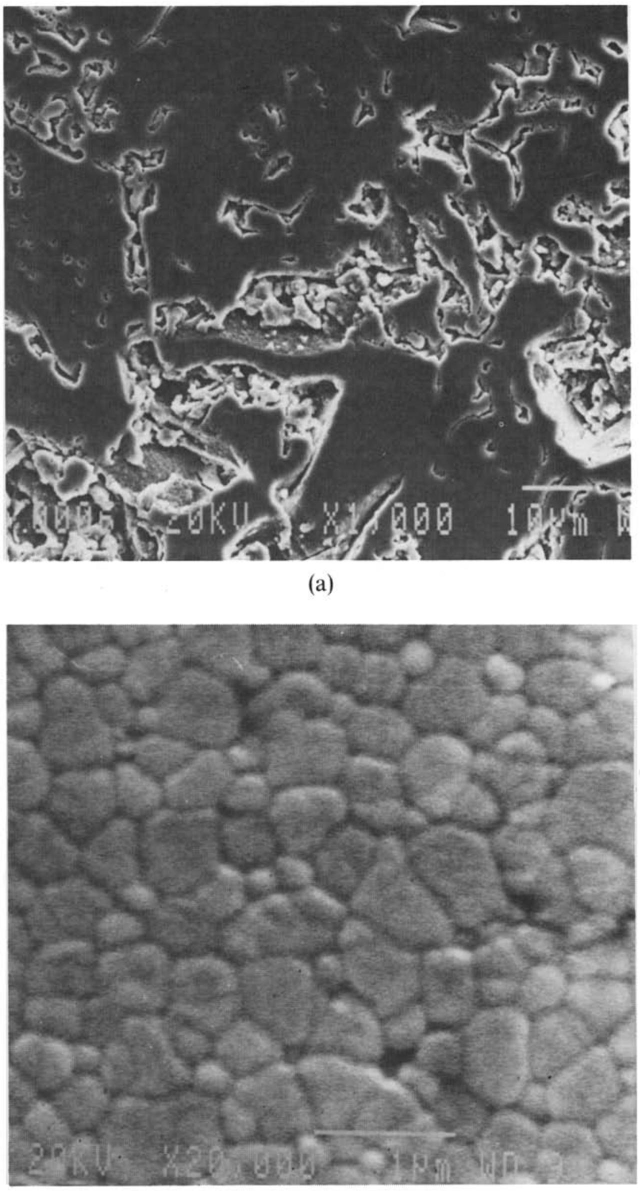

(a)

(b)

Fig. 16. SEM micrograph of polished surface of sample A900 sintered for 3 h at 1500°C: (a) showing an intergranular porosity; (b) showing an intraaggregate homogeneous sintering.

4 Conclusion

The preceding results show that when dense sintered materials are required, the synthesis of acetate precursors has to be carried out without any dilution of the starting material (commercial zirconyl acetate solution containing 320 g/litre in ZrO_2) and using ammonia with concentration in the range 1·3 to 2·8 mol/litre. Increase in the ammonia concentration up to 3·8 mol/litre seemed to decrease the hardness of agglomerates in zirconia powders obtained by pyrolysis at 900°C, but it also decreased the densities of green and sintered materials.

Even in the best conditions, relatively poor densities were achieved, namely 78% by sintering at 1500°C and 85% by sintering at 1600°C for 3 h. This is explained by the presence, in the white zirconia powders formed by pyrolysis at 900°C, of residual carbon in the form of carbonate or oxycarbonate groups which decompose at temperatures between 900 and 1500°C.

References

1. Heuer, A. H. & Hobbs, L. W. (eds), *Science and Technology of Zirconia, Advances in Ceramics*, Vol. 3, 1981.
2. Glaussen, N., Ruhle, M. & Heuer, A. H. (eds), *Science and Technology of Zirconia II, Advances in Ceramics*, Vol. 12, 1984.
3. Somiya, S., Yamamoko, N. & Yanagida, H. (eds), *Science and Technology of Zirconia III, Advances in Ceramics*, Vol. 24, 1988.
4. Jebrouni, M., Durand, B. & Roubin, M., Elaboration de zircone pure par reaction en milieu nitrate fondu et caractérisation. *Ann. Chim. Fr.*, **16** (1991) 569–79.
5. Samdi, A., Grollier-Baron, Th., Durand, B. & Roubin, M., (a) Elaboration de poudres finement divisées de zircone pure à partir d'acétate de zirconium cristallisé. *Ann. Chim. Fr.*, **13** (1988) 171–87. (b) Elaboration de poudres finement divisées de zircone pure à partir d'acétate de zirconium amorphes. *Ann. Chim. Fr.*, **13** (1988) 471–82.
6. Bernstein, E., Blanchin, M. G. & Samdi, A., Structural characteristics of ZrO_2 powders prepared from acetates. *Ceram. Int.*, **15** (1989) 337–43.
7. Samdi, A., Grollier-Baron, Th., Durand, B. & Roubin, M., (a) Analyse des solides pulvérulents formés par cristallisation en milieu acide acétique concentré de solutions renfermant du zirconium de l'yttrium. *Ann. Chim. Fr.*, **13** (1988) 483–8. (b) Préparation, par hydrolyse de solutions aqueuses, d'acétate de zirconium et d'yttrium précurseurs de zircones dopées à l'yttrium finement divisées. *Ann. Chim. Fr.*, **13** (1988) 517–26.
8. Klug, H. P. & Alexander, L. E., *X-Ray Diffraction Procedure*. John Wiley and Sons, Ind., New York, 1954, pp. 509–10.
9. Samdi, A., Grollier-Baron, Th., Durand, B. & Roubin, M., Etude des conditions de dispersion optimale de poudres de zircone obtenues par pyrolyse d'acétates de zirconium. *Powder Technology*, **66** (1991) 237–42.
10. AFNOR, French normalization, Powder metallurgy Determination of tap density, NF A 95-112 (equivalence with ISO 3953-1977).
11. Frey, R. G. & Halloran, J. W., Compaction behavior of spray dried alumina. *J. Amer. Ceram. Soc.*, **67**(3) (1984) 199–203.
12. Van de Graaf, M. A. C. G., Ter Maat, J. H. H. & Gurgraaf, A. J., Microstructural development during pressing and sintering of ultrafine zirconia powders. In *Ceramic Powders*, Elsevier, Amsterdam, 1983, pp. 783–94.
13. Massin, G. L., Markhoff, C. J. & McCoy, L. G., Characterization of ceramic powder compaction. *Ceram. Bull.*, **61**(8) (1982) 857–60.
14. Matsumoto, R. L. K., Analysis of powder compaction using a compaction rate diagram. *J. Amer. Ceram. Soc.*, **73**(2) (1990) 465–8.
15. Dimilia, R. A. & Reed, J. S., Dependence of compaction on the glass transition temperature on the binder phase. *Ceram. Bull.*, **62**(4) (1983) 484–8.
16. Zheng, J. & Reed, J. S., Particle and granule parameter affecting compaction efficiency in dry pressing. *J. Amer. Ceram. Soc.*, **71**(11) (1988) C456–C458.
17. Descemond, M., Durand, B., Samdi, A., Brodhag, C. Thevenot, F. & Roubin, M., Influence of elaboration conditions on the densification of zirconia powders obtained from acetates. *J. Mat. Sci.*, **28** (1993) 3754–60.
18. Bennison, S. J. & Harmer, M. P., Swelling of hot-pressed Al_2O_3. *J. Amer. Ceram. Soc.*, **68**(11) (1985) 591–7.
19. Dogan, F., Roosen, A. & Hausner, H., Influence of hydroxide precursor processing in the densification of yttrium oxide powders. In *Advances in Ceramics*, Vol. 21, *Ceramic Powder Science*, ed. G. L. Messing, K. S. Mazdiyasni, J. W. McCauley & R. A. Haber. The American Ceramic Society Inc., Westerville, Ohio, 1987, pp. 681–9.
20. Kang, S.-J. L. & Yoon, K. J., Densification of ceramics containing entrapped gases. *J. Eur. Ceram. Soc.*, **5** (1989) 135–9.
21. Smith, A., Baumard, J. F., Sinterability of tetragonal ZrO_2 powders. *Am. Ceram. Soc. Bull.*, **66**(7) (1987) 1144–8.
22. Kim, D. H. & Kim, C. H., Entrapped gas effect in the fast firing of yttria-doped zirconia. *J. Am. Ceram. Soc.*, **75**(3) (1992) 716–18.